ISSN 1561-8323 (Print)
ISSN 2524-2431 (Online)

ФИЗИКА

PHYSICS

UDC 535.34:546.23:546.28
https://doi.org/10.29235/1561-8323-2024-68-2-112-117

Received 18.03.2024
Поступило в редакцию 18.03.2024

Ting Wang[1], Academician Fadei F. Komarov[2], Irina N. Parkhomenko[1], Guofeng Yang[3], Junjun Xue[4]

[1]Belarusian State University, Minsk, Republic of Belarus
[2]A. N. Sevchenko Institute of Applied Physical Problems of Belarusian State University, Minsk, Republic of Belarus
[3]School of Science, Jiangnan University, Wuxi, China
[4]College of Electronic and Optical Engineering & College of Flexible Electronics (Future Technology), Nanjing University of Posts and Telecommunications, Nanjing, China

SILICON HYPERDOPING USING SELENIUM AND MANGANESE ION IMPLANTATION AND PULSED LASER ANNEALING

Abstract. The effect of pulsed laser annealing (PLA) on the structure and optical properties of Mn-, Se- and (Mn+Se)-implanted silicon layers was studied. 95 keV Mn^+ and 200 keV Se^+ ions were implanted separately and together into p-type Si wafers up to the fluence $1 \cdot 10^{16}$ cm^{-2} at room temperature. Then, the samples were irradiated in the ambient air with a single 2 J/cm^2 ruby laser pulse. The detailed redistribution of Mn and Se atoms in the implanted layers during PLA was examined using Rutherford backscattering spectroscopy in random and channeling configuration. It was found that a notable percentage of implanted manganese atoms diffuses to the silicon surface, while the Se concentration depth profile broadens in both directions after PLA. Mn co-implantation enhances the Se diffusion to the surface, which leads to a Se decrease in crystalline silicon, but it does improve the crystal structure of the implanted silicon layer due to the increase of diffusion velocity. In contrast to the Mn-implanted sample, Se-implanted and (Mn+Se)-co-implanted samples after PLA exhibit strong optical absorption in the infrared range. The observed band at 0.6 eV is associated with electronic transitions from the intermediate band to the lowest energy levels of the conduction band.

Keywords: silicon, hyperdoping, selenium and manganese implantation, laser annealing, impurity sub-band, absorptance

For citation. Ting Wang, Komarov F. F., Parkhomenko I. N., Guofeng Yang, Junjun Xue. Silicon hyperdoping using selenium and manganese ion implantation and pulsed laser annealing. *Doklady Natsional'noi akademii nauk Belarusi = Doklady of the National Academy of Sciences of Belarus*, 2024, vol. 68, no. 2, pp. 112–117. https://doi.org/10.29235/1561-8323-2024-68-2-112-117

Тин Ван[1], академик Ф. Ф. Комаров[2], И. Н. Пархоменко[1], Гофэн Ян[3], Цзюньцзюнь Сюэ[4]

[1]Белорусский государственный университет, Минск, Республика Беларусь
[2]Институт прикладных физических проблем им. А. Н. Севченко Белорусского государственного университета, Минск, Республика Беларусь
[3]Школа науки, Цзяннаньский университет, Уси, Китайская Народная Республика
[4]Школа электронной и оптической инженерии и Школа гибкой электроники (Технологии будущего), Нанкинский университет почты и телекоммуникаций, Нанкин, Китайская Народная Республика

ГИПЕРДОПИРОВАНИЕ КРЕМНИЯ С ПОМОЩЬЮ ИМПЛАНТАЦИИ ИОНОВ СЕЛЕНА И МАРГАНЦА И ИМПУЛЬСНОГО ЛАЗЕРНОГО ОТЖИГА

Аннотация. Изучено влияние импульсного лазерного отжига (ИЛО) на структуру и оптические свойства имплантированных ионами Mn-, Se- и (Mn+Se)-слоев кремния. Ионы Mn^+ с энергией 95 кэВ и Se^+ с энергией 200 кэВ отдельно и совместно были имплантированы в пластины Si *p*-типа равными флюенсами $1 \cdot 10^{16}$ $см^{-2}$ при комнатной температуре. Затем образцы облучались импульсами рубинового лазера с плотностью энергии 2 Дж/$см^2$. Детальное перераспределение атомов Mn и Se в имплантированных слоях при ИЛО исследовалось с помощью случайных и каналированных спектров резерфордовского обратного рассеяния. Было обнаружено, что значительный процент имплантированного марганца диффундирует к поверхности кремния, а концентрационный профиль Se по глубине уширяется как к поверхности, так и в глубь образца в течение ИЛО. Совместная имплантация Mn усиливает диффузию Se к поверхности, уменьшает активацию Se в кристаллическом кремнии, но улучшает кристаллическую

структуру имплантированного слоя кремния. В отличие от образцов, имплантированных только Mn, Se-имплантированные и (Mn+Se)-коимплантированные образцы после ИЛО демонстрируют сильное оптическое поглощение в инфракрасном диапазоне. Наблюдаемая полоса поглощения при 0,6 эВ связана с электронными переходами между сформированной подзоной и нижними энергетическими уровнями зоны проводимости.

Ключевые слова: кремний, гипердопирование, имплантация селена и марганца, лазерный отжиг, подзона, поглощение

Для цитирования. Гипердопирование кремния с помощью имплантации ионов селена и марганца и импульсного лазерного отжига / Тин Ван [и др.] // Докл. Нац. акад. наук Беларуси. – 2024. – Т. 68, № 2. – С. 112–117. https://doi.org/10.29235/1561-8323-2024-68-2-112-117

Introduction. Silicon is the most commonly used semiconductor in microelectronics and optoelectronics. Due to the large band gap (1.12 eV), the optical advantages of silicon are eliminated in the IR range (>1.1 μm). Specifically, silicon photodetectors are insensitive at three main fiber-optic communication wavelength bands: *S*, *C* and *L* [1]. The equilibrium solubility of chalcogens (S, Se, Te) in silicon is ~10^{16} cm^{-3}. Such concentrations of chalcogen atoms lead to the formation of deep levels in the silicon band gap. However, impurity levels merge into a subband at supersaturation (concentrations exceeded by 4–5 orders above the equilibrium solid solubility concentration). Hyperdoping is currently being used to engineer new materials with unique and exotic properties. Silicon hyperdoped with chalcogens exhibits strong subband gap absorption down to photon energies as low as 0.5 eV [2]. To realize hyperdoping above the solid solubility limits, nonequilibrium methods such as ion implantation followed by femto-, pico-, and nanosecond laser pulses [3–5] or flash-lamp annealing were used.

The properties of 3d transition-metal impurities in silicon have attracted growing interest in recent years. Being fast diffusers in silicon, they influence the performance of silicon devices if introduced unintentionally. Mn is one of the 3d transition metals, and it diffuses interstitially into silicon at a high temperature, and most of it can remain at the interstitial site after quenching from high temperature [6]. On the other hand, higher Mn silicides are promising materials for applications in optoelectronics, spintronics, and thermoelectrics due to their interesting physical and chemical properties, e.g., the direct band gap in the infrared region, ferromagnetism with relatively large magnetic moment, large Seebeck coefficient, and high resistance to oxidation at high temperatures [7].

This work reports on the fabrication of Se-hyperdoped silicon layers using ion implantation followed by pulsed laser annealing (PLA) and with the assist with Mn^+. We focus on the structural and optical properties of the Mn-implanted and Se-implanted layers and coimplanted with (Mn+Se) ions silicon layers after PLA. These results may contribute to the development of optoelectronic devices and related technologies.

Materials and methods of research. *P*-Si <111> KDB 10 wafers (2 × 2 cm^2) were separately implanted with 200 keV Se^+ and 95 keV Mn^+ ions to the fluence of $1 \cdot 10^{16}$ ions/cm^2 at room temperature. One of the Mn-implanted samples was then co-implanted with 200 keV Se^+ ions at the same fluence ($1 \cdot 10^{16}$ cm^{-2}). Some of the as-implanted samples were subjected to PLA using a ruby laser single pulse with λ = 694 nm and a full width at half maximum 70 ns. The laser beam had been homogenized to a beam spot with a diameter of 4 mm. The energy density in the laser pulse was set as 2 J/cm^2.

The Mn and Se concentration depth distribution profiles, fraction of impurities at lattice sites, and Si crystallinity of the implanted and annealed samples were analyzed by Rutherford backscattering spectroscopy in random (RBS/R) and channeling directions (RBS/C) using 1.5 MeV He^+ ions. The impurity concentration profiles were extracted from the RBS/R spectra using HEAD software. The RBS spectra were simulated using this software stepwise until complete overlap with the experimental spectra was achieved. For comparison the Mn and Se depth profiles were calculated with the SRIM-2013 code [8].

To investigate the crystalline quality of the modified silicon layers, Raman spectroscopy measurements were performed in backscattering geometry with a Ramanor U1000 (Jobin Yvon) spectrometer using a 532 nm laser beam as the excitation source.

The optical properties of the samples were investigated by measurements of the transmittance (*T*) and specular reflectance (*R*) spectra using a Lambda 1050 UV/Vis/NIR spectrometer. The specular reflectance spectra were measured at an 8° incident angle using a Universal Reflectance Accessory with an accuracy of 0.1 %. Absorptance spectra were calculated using the following formula:

$$A = 100\ \% - R - T.$$

Results and discussion. Fig. 1 shows the RBS spectra of the annealed implanted samples in random and channeling regimes.

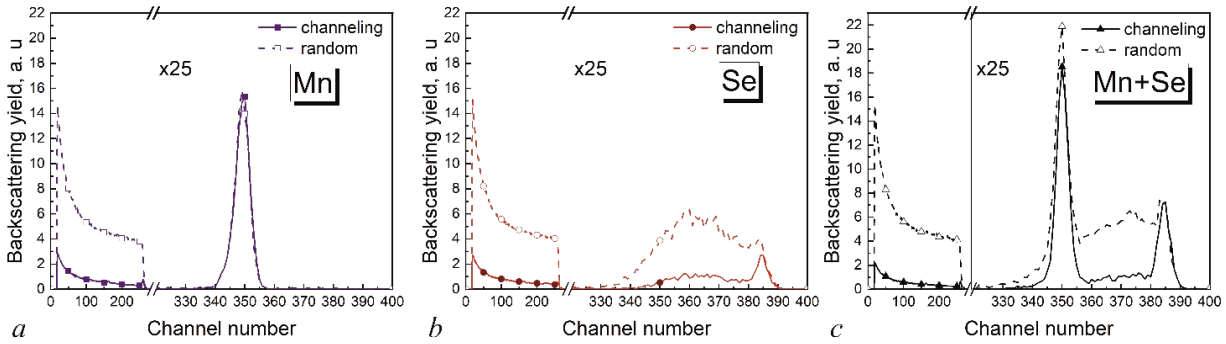

Fig. 1. Channeling and random RBS spectra of the samples implanted with Mn (*a*), Se (*b*) and Mn+Se (*c*) after PLA

To estimate the restoration of disordered implanted silicon surfaces after PLA and the degree of substitution of Se, the values of χ_{Si} and χ_{Se} were used. These values represent integral channeled-to-random ratios in channels associated with Si (channels 150–275) and embedded impurities (Se) (channels 300–400), respectively. For perfect bulk silicon, χ_{min}^{Si} is equal to 0.05. The degree of crystallinity of the implanted layer (f_{cr}) was determined using the formula

$$f_{cr} = \frac{1-\chi_{Si}}{1-\chi_{min}^{Si}}. \quad (1)$$

The fraction of impurity atoms in the silicon lattice sites f_{subst} was calculated using the formula from the work [9]:

$$f_{Se\,subst} = \frac{1-\chi_{Se}}{1-\chi_{min}^{Se}}. \quad (2)$$

The corresponding calculated values are given in Table.

The degree of Si crystallinity and Se substitutional fraction in silicon for the implanted layers

Implanted ions	$1-\chi_{Si}$	$1-\chi_i$	f_{cr}, %	$f_{Se\,subst}$, %
Mn^+	0.893	0.038	94.0	–
Se^+	0.888	0.781	93.5	86.0
$Mn^+ + Se^+$	0.924	0.634	97.2	67.0

In the case of Mn implantation, PLA causes fast Mn diffusion to the surface, and there is no difference between the aligned and random spectra. This suggests that no lattice Mn incorporation occurs. In contrast to Mn, Se substitutional incorporation occurs after PLA up to 86 and 67 % for the Se- and (Mn+Se)-implanted samples, respectively. Thus, the preliminary Mn implantation affects Se substitution in silicon. However, the annealed (Mn+Se)-implanted sample stands out by the best extent of restoration of the silicon crystal structure.

Fig. 2 shows the Mn and Se depth profiles extracted from the RBS spectra and simulated ones using SRIM code. In the case of the samples as-implanted with one type of ions, the maxima of Mn and Se concentration slightly shift to the surface and deep into, respectively, compared with the corresponding SRIM simulated ones. However, the maximum of the Se concentration profile slightly shifts also to the surface for the sample co-implanted with (Mn+Se).

PLA results in a significant diffusion of Mn to the subsurface layer (50 nm) for Mn-implanted sample. In the case of the sample implanted with (Mn+Se), after PLA, the out-diffusion of Mn increases, but a certain amount of Mn impurities (>0.5 %) remains at a depth of up to 120 nm. In the case of the Se-implanted sample, PLA leads to a considerable Se redistribution toward the surface and into the bulk. The presence of Mn atoms in the implanted sample enhances diffusion of Se atoms to the surface. The

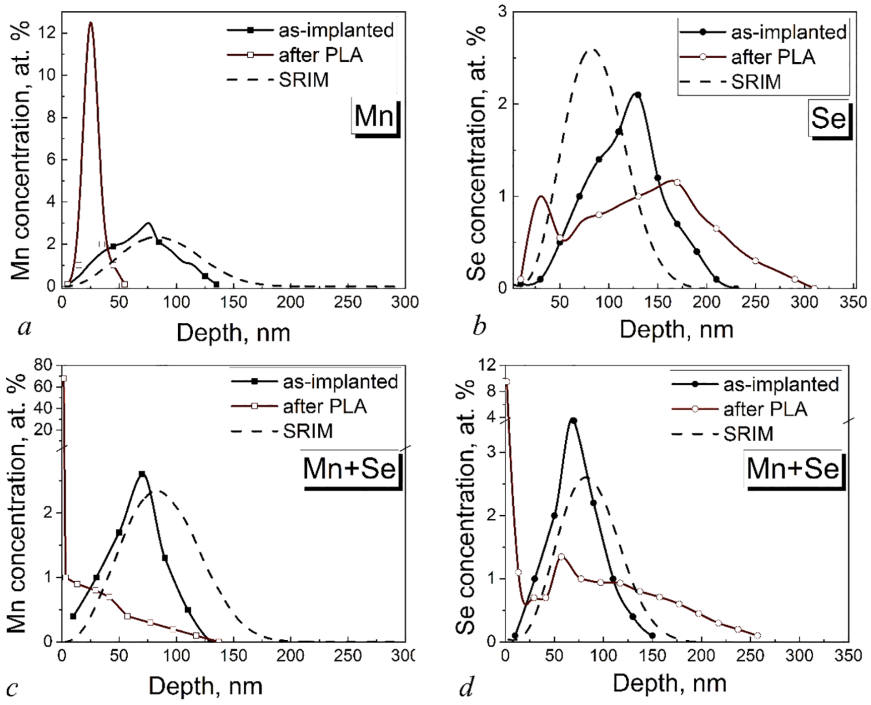

Fig. 2. Depth distribution of Mn (*a*, *c*) and Se (*b*, *d*) concentrations of the sample implanted with Mn (*a*), Se (*b*) and Mn+Se (*c*, *d*)

thickness of layer embedded with Se atoms after PLA extended to 250 and 300 nm depth with and without Mn presence, respectively.

In silicon, Mn atoms have much bigger diffusion coefficient (10^{-6} cm^2/s [10]) than Se atoms ($8.6 \cdot 10^{-10}$ cm^2/s [11]). As we can see from Fig. 1, the existence of Mn does improve the diffusion velocity of Se in silicon. Although the increase of diffusion coefficient leads to more ions diffuse to the surface, it does bring a more uniform diffusion rate, which makes the ion distribution in silicon more uniform and improves the crystal structure. At the same time, the existence of Se atoms slows down the diffusional mobility of Mn atoms. Therefore, Mn atoms itself diffused deeper in the silicon substrate.

Fig. 3 shows the Raman spectra of the as-implanted and annealed samples. It should be noted that the signal from the amorphous Si at 480 cm^{-1} did not manifest itself in the spectra of the as-implanted samples. However, in the case of the Se-implanted sample, the Raman spectrum exhibits a band at 509 cm^{-1} which is attributed to silicon under tensile stress. The stress level is about 5 GPa [12]. The spectrum of the sample implanted with Mn+Se exhibits a band with maximum at 519 cm^{-1} (~0.7 GPa) with the Si band shoulder at lower wavenumbers. Thus, Mn co-implantation suppresses the formation of Si layer with tensile stress. Subsequent PLA substantially improves the crystallinity of the implanted layers. In contrast to the Mn-implanted sample, the spectra of samples implanted with Se and Mn+Se exhibit Si band shoulder at lower wavenumbers. It assigns with the incorporation of Se in the silicon matrix. Based on the Raman spectra, the perfection of crystal structure of Se and Mn+Se samples after PLA is similar.

According to the RBS data, the average concentration of Se atoms in a 200 nm thick silicon layer after PLA is ~$4 \cdot 10^{20}$ cm^{-3} for the Se-implanted sample. The concentration of Se atoms substituting silicon lattice atoms in the doped region is $3.4 \cdot 10^{20}$ cm^{-3}. The rest of the implanted impurities is in the form of polyatomic clusters [13] or segregated to the sample surface. We use the Mott theory to estimate the possibility of an acquired concentration of Se atoms to form an impurity sub-band in the silicon [14]. The critical concentration of donor electrons N_{cr} for the insulator-to-metal transition (IMT) in group-IV semiconductors can be estimated using the following formula [15]

$$N_{cr}^{1/3} a_B^* = 0.25,$$

a_H^* is the first Bohr radius of the donor electrons. The first Bohr radius can be represented as [16]

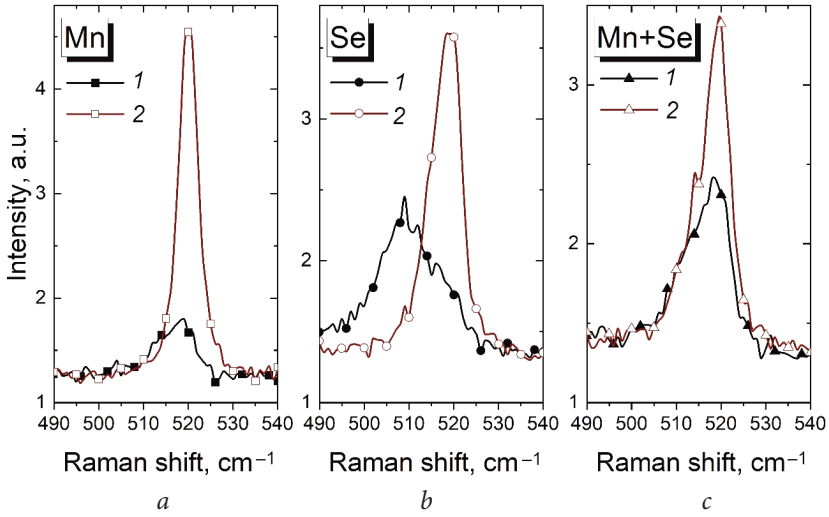

Fig. 3. Raman spectra of the samples implanted with Mn (*a*), Se (*b*) and Mn+Se (*c*) before (*1*) and after (*2*) PLA

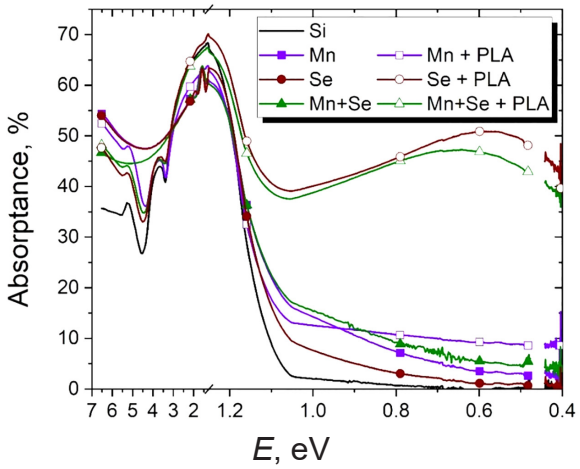

Fig. 4. Absorptance spectra of the sample implanted with Mn, Se and Mn+Se before and after PLA

$$a_B^* = \frac{e^2}{8\pi\varepsilon_0\varepsilon_r E_d},$$

where e is the electron charge, ε_0 is the dielectric permittivity of vacuum, ε_r is the high-frequency dielectric permittivity of silicon, and E_d is the activation energy of the localized states. Taking into account the value of activation energy E_d = 0.307 eV for selenium atoms in the silicon lattice [1], the isotropic Bohr radius by the Mott criterion is 2.023 Å. Therefore, the critical dopant concentration for providing an insulator-metal transition in Se-hyperdoped silicon is ~$9.5 \cdot 10^{20}$ cm^{-3}. For the silicon doping level ($4 \cdot 10^{20}$ cm^{-3}) obtained in this study, this transition has not yet been reached.

Fig. 4 shows the absorptance spectra of the implanted silicon before and after PLA. In the case of the Mn-implanted layer, PLA results in the 6–8 % increase of absorptance in NIR spectral range, whereas the absorptance for Se- and (Mn+Se)-implanted silicon increased by up to 50 and 40 %, respectively. As can be seen from this figure, the incorporation of Se after PLA results in the formation of wide band in the NIR range with the maximum at 0.57 and 0.64 eV for Se- and (Mn+Se)-implanted silicon, respectively. It correlates with the activation energy of the Se deep donor level in Si (E_c – 0.593 eV) [17]. The smaller energetic position of the maximum of the NIR band for the Se-implanted sample is explained by the higher fraction of Se atoms in substitutional lattice sites.

Conclusions. Se-hyperdoped silicon layers with an average concentration of approximately 1 at.% were formed by the implantation of Se ions and by co-implantation of (Mn+Se) ions followed by nanosecond laser annealing at an energy density in pulse of 2 J/cm^2. Preliminary Mn implantation decreases the Se substitutional fraction in silicon lattice, but enhances the restoration of the Si crystal structure via PLA. Se-hyperdoped silicon layers demonstrate effective absorptance in the NIR range (up to 50 %), which is caused by the formation of an impurity sub-band in the silicon band gap at approximately 0.6 eV below the conduction band. Future experiments will provide additional insights into the unusual optical and electronic properties that can be achieved in silicon supersaturated with Se using ion-implantation and pulsed laser annealing.

References

1. Carey J. E., Crouch C. H., Shen M., Mazur E. Visible and near-infrared responsivity of femtosecond-laser microstructured silicon photodiodes. *Optics Letters*, 2005, vol. 30, no. 14, pp. 1773–1775. https://doi.org/10.1364/ol.30.001773

2. Ertekin E., Winkler M. T., Recht D., Said A. J., Aziz M. J., Buonassisi T., Grossman J. C. Insulator-to-metal transition in selenium-hyperdoped silicon: observation and origin. *Physical Review Letters*, 2012, vol. 108, no. 2, art. 026401. https://doi.org/10.1103/physrevlett.108.026401

3. Komarov F., Ivlev G., Zayats G., Komarov A., Nechaev N., Parkhomenko I., Vlasukova L., Wendler E., Miskiewicz S. Experimental study and modeling of silicon supersaturated with selenium by ion implantation and nanosecond-laser melting. *Acta Physica Polonica A*, 2019, vol. 136, no. 2, pp. 254–259. https://doi.org/10.12693/aphyspola.136.254

4. Komarov F. F., Nechaev N. S., Ivlev G. D., Vlasukova L. A., Parkhomenko I. N., Wendler E., Romanov I. A., Berencén Y., Pilko V. V., Zhigulin D. V., Komarov A. F. Structural and optical properties of Si hyperdoped with Te by ion implantation and pulsed laser annealing. *Vacuum*, 2020, vol. 178, art. 109434. https://doi.org/10.1016/j.vacuum.2020.109434

5. Yang W., Lim S. Q., Williams J. S. Chapter 8 – Optical hyperdoping. Cristiano F., La Magna A. (eds.). *Laser Annealing Processes in Semiconductor Technology*. Cambridge, Woodhead Publishing, 2021, pp. 353–356. https://doi.org/10.1016/c2019-0-01254-x

6. Nakashima H., Hashimoto K. Deep impurity levels and diffusion coefficient of manganese in silicon. *Journal of Applied Physics*, 1991, vol. 69, no. 3, pp. 1440–1445. https://doi.org/10.1063/1.347285

7. Naito M., Nakanishi R., Machida N., Shigematsu T., Ishimaru M., Valdez J. A., Sickafus K. E. Growth of higher manganese silicides from amorphous manganese-silicon layers synthesized by ion implantation. *Nuclear Instruments and Methods in Physics Research Section B: Beam Interactions with Materials and Atoms*, 2012, vol. 272, no. 1, pp. 446–449. https://doi.org/10.1016/j.nimb.2011.01.120

8. Ziegler J. F., Ziegler M. D., Biersack J. P. SRIM – The stopping and range of ions in matter. *Nuclear Instruments and Methods in Physics Research Section B: Beam Interactions with Materials and Atoms*, 2010, vol. 268, no. 11–12, pp. 1818–1823. https://doi.org/10.1016/j.nimb.2010.02.091

9. Feldman L. C., Mayer J. W., Picraux S. T. *Materials analysis by ion channeling: submicron crystallography.* Academic Press, 2012. 320 p.

10. Weber E. R. Transition metals in silicon. *Applied Physics A*, 1983, vol. 30, pp. 1–22. https://doi.org/10.1007/bf00617708

11. Stümpel H., Vorderwülbecke M., Mimkes J. Diffusion of selenium and tellurium in silicon. *Applied Physics A*, 1988, vol. 46, pp 159–163. https://doi.org/10.1007/bf00939258

12. Poborchii V., Tada T., Kanayama T. Study of stress in a shallow-trench-isolated Si structure using polarized confocal near-UV Raman microscopy of its cross section. *Applied Physics Letters*, 2007, vol. 91, no. 24, art. 241902. https://doi.org/10.1063/1.2825286

13. Haberfehlner G., Smith M. J., Idrobo J.-C., Auvert G., Sher M.-J., Winkler M. T., Mazur E., Gambacorti N., Gradečak S., Bleuet P. Selenium segregation in femtosecond-laser hyperdoped silicon revealed by electron tomography. *Microscopy and Microanalysis*, 2013, vol. 19, no. 3, pp. 716–725. https://doi.org/10.1017/s1431927613000342

14. Mott N. F. Metal-insulator transitions. *Contemporary Physics*, 1973, vol. 14, no. 5, pp. 401–413. https://doi.org/10.1080/00107517308210764

15. Schubert E. F. *Doping in III–V semiconductors*. Cambridge, Cambridge University Press, 1993. 606 p. https://doi.org/10.1017/cbo9780511599828

16. Zhou S., Liu F., Prucnal S., Gao K., Khalid M., Baehtz C., Posselt M., Skorupa W., Helm M. Hyperdoping silicon with selenium: solid vs. liquid phase epitaxy. *Scientific Reports*, 2015, vol. 5, no. 1, pp. 1773–1775. https://doi.org/10.1038/srep08329

17. Janzén E., Stedman R., Grossmann G., Grimmeiss H. G. High-resolution studies of sulfur- and selenium-related donor centers in silicon. *Physical Review B*, 1984, vol. 29, no. 4, pp. 1907–1918. https://doi.org/10.1103/physrevb.29.1907

Information about the authors

Ting Wang – Postgraduate Student. Belarusian State University (4, Nezavisimosti Ave., 220030, Minsk, Republic of Belarus). E-mail: tingwang@bsu.by.

Komarov Fadei F. – Academician, D. Sc. (Physics and Mathematics), Professor. A. N. Sevchenko Institute of Applied Physical Problems of the Belarusian State University (7, Kurchatov Str., 220045, Minsk, Republic of Belarus). E-mail: komarovf@bsu.by.

Parkhomenko Irina N. – Ph. D. (Physics and Mathematics), Leading Researcher. Belarusian State University (5, Kurchatov Str., 220108, Minsk, Republic of Belarus). E-mail: parkhomenko@bsu.by.

Guofeng Yang – D. Sc., Professor. School of Science, Jiangsu Provincial Research Center of Light Industrial Optoelectronic Engineering and Technology, Jiangnan University (1800, Lihu Avenue, 214122, Wuxi, China). E-mail: gfyang@jiangnan.edu.cn.

Junjun Xue – Ph. D., Associate Professor. College of Electronic and Optical Engineering & College of Flexible Electronics (Future Technology), Nanjing University of Posts and Telecommunications (9, Wenyuan Road, 210023, Nanjing, China). E-mail: jjxue@njupt.edu.cn.

Информация об авторах

Ван Тин – аспирант. Белорусский государственный университет (пр. Независимости, 4, 220030, Минск, Республика Беларусь). E-mail: tingwang@bsu.by.

Комаров Фадей Фадеевич – академик, д-р физ.-мат. наук, профессор. Институт прикладных физических проблем им. А. Н. Севченко БГУ (ул. Курчатова, 7, 220045, Минск, Республика Беларусь). E-mail: komarovf@bsu.by.

Пархоменко Ирина Николаевна – канд. физ.-мат. наук, вед. науч. сотрудник. Белорусский государственный университет (ул. Курчатова, 5, 220045, Минск, Республика Беларусь). E-mail: parkhomenko@bsu.by.

Гофэн Ян – д-р наук, профессор. Школа науки, Провинциальный исследовательский центр оптико-электронной техники и технологий легкой промышленности провинции Цзянсу, Цзяннаньский университет (214122, Уси, Китай, проспект Лиху, 1800). E-mail: gfyang@jiangnan.edu.cn.

Цзюньцзюнь Сюэ – канд. наук, доцент. Школа электронной и оптической инженерии и школа гибкой электроники (Технологии будущего) Нанкинского университета почты и телекоммуникаций (улица Вэньюань, 9, 210023, Нанкин, Китай). E-mail: jjxue@njupt.edu.cn.